The parabolic focal conic : a new smectic a defect

Ch. S. Rosenblatt, R. Pindak, N.A. Clark, R.B. Meyer

Classification
Physics Abstracts
61.30 — 61.70

THE PARABOLIC FOCAL CONIC : A NEW SMECTIC A DEFECT

Ch. S. ROSENBLATT, R. PINDAK,
N. A. CLARK and R. B. MEYER

Gordon McKay Laboratory, Division of Applied Sciences, Harvard University
Cambridge, Massachusetts 02138, U.S.A.

(*Reçu le 14 mars 1977, accepté le 31 mai 1977*)

Résumé. — Le cas spécial d'un domaine focal dans lequel les lignes forment une paire de paraboles focales (un *domaine focal parabolique*) est observé dans la phase smectique A du composé cyanobenzylidène octyloxyaniline. La géométrie de ces défauts est étudiée et utilisée pour déterminer les interactions qu'ils ont soit avec les surfaces frontières, soit entre eux. On montre que la texture polygonale obtenue par dilatation d'une structure plane d'un smectique A ou cholestérique est un réseau de domaines focaux paraboliques. La génération et la structure de ces réseaux sont discutées.

Abstract. — The special case of a focal conic defect in which the line discontinuities form a pair of confocal parabolae (a parabolic focal conic) has been observed in smectic A cyanobenzylidene octyloxyaniline. The geometry of these defects has been studied and used to determine their interactions with bounding surfaces and with each other. The polygonal texture obtained by dilation of smectic A and cholesteric plane textures is shown to be an array of parabolic focal conic defects. The generation and structure of such arrays will be discussed.

1. **Introduction.** — The smectic A phase may be described as a stack of two-dimensional liquid layers, which are easily curved and flow over one another, but whose thickness is nearly constant. The rod-like molecules comprising this phase have their long axis oriented normal to the layers. This makes the system optically uniaxial, with a large anisotropy in the index of refraction.

The textures formed by this phase depend critically on the kinds of defects it can contain. If one assumes that the layers are well defined with precisely constant thickness, and that they are curved smoothly except at a system of line defects along which cusps in the curvature can occur, then, by classical geometrical arguments, one can show that the line defects must occur as pairs of confocal ellipses and hyperbolae. The associated smectic layers form a family of surfaces known as Dupin cyclides, the singularities of which are the cusps whose loci form the confocal line defects [1, 2]. Their characteristic geometrical form was an early clue to the underlying layer structure of this phase. Although the geometry of an isolated confocal pair of defects is known, fundamental problems concerning focal conics and defects in smectic A samples remain unsolved. These include understanding the structure of complex arrays of defects which are observed in smectic A samples and mechanisms of generation of focal conics. In this paper we address these questions.

Theoretical studies [3] of the problem of filling three-dimensional space or a bounded slab of smectic material with an array of focal conic defects have produced predictions which do not agree well with observations, and simply do not predict the full range of observed behaviour. For example, in experiments which start with planar texture smectic A or cholesteric samples and proceed by deforming them under a dilative stress normal to the layers, one observes a sequence of elastic and plastic strain patterns which finally appear as a polygonal array of focal conic defect lines. Intuitively it appears that within a given volume of the sample the observed defect structure can relax the small internal strain to a nearly dilation free structure (with a minimum energy). Following the lead of F. Grandjean and G. Friedel, Bouligand has made elegant geometrical analyses of observed polygonal focal conic textures in long pitch cholesterics [4] which have done much to clarify some of these structures. The specific details of Bouligand's models, however, require a large layer tilt relative to the initial planar geometry. That is allowed by the very weak anchoring of the cholesteric helix at the glass plates, whereas in our sample the anchoring of the smectic layers seems to be strong. Moreover, we find

that the polygonal texture appears at very small sample dilation, suggesting that it involves only small rearrangements of the molecules from their initial structure, rather than large reorientations. We will propose in this paper a different defect structure which produces a polygonal array, and which is compatible with small dilation of the sample and small deviation from a planar texture.

We begin by describing observations of a particular defect structure which appears to be a limiting case of the focal conic form in which each of the two lines is a parabola passing through the other's focus. We refer to these defects as parabolic focal conics (PFC's). These structures fit into the general scheme described in the preceding paragraph and appear to be a principal dilative strain relaxation mechanism in planar samples. In the next section we describe our observations. We then discuss the ideal confocal PFC structure. Finally, we consider how these defects interact with one another and with the sample surfaces, how they fill space, and how they relieve dilative strains of initially perfect planar textures.

2. **Observations.** — 2.1 SAMPLE PREPARATION. — Observations were made on single domain smectic A samples of cyanobenzylidene octyloxyaniline (CBOOA) in both the parallel and perpendicular geometries by means of polarized optical transmission microscopy. (By *parallel* we mean that the long molecular axis is parallel to some unique direction in the plane of the glass slides containing the sample. By *perpendicular* we mean it is perpendicular to the slides.) The slide surfaces were treated for parallel orientation by oblique evaporation of a 100 Å thick striated SiO layer. For perpendicular alignment, the surfactant hexadecyltrimethylammonium bromide (HTAB) was used. The CBOOA was obtained from Eastman Kodak and was not further purified. In the smectic A phase excellent alignment was obtained upon cooling from the nematic phase, as long as the sample was not permitted to crystallize between the slides. Crystallization always degraded the orienting ability of the SiO and HTAB, leading to incomplete extinction between crossed polarizers.

2.2 PARALLEL GEOMETRY. — Two types of focal conic defects were observed in parallel samples. The familiar cylindrically symmetric form [1] with line defects consisting of a circle parallel to the undisturbed layers and a straight line passing through the center of the circle was occasionally found. However, the far more numerous and more easily generated defect structure appeared as lines in the form of various sized *wish-bones*, oriented with their tails normal to the undisturbed layers (Fig. 1) and appearing under the application of a dilative strain. In an effort to characterize these defects quantitatively, measurements of the wishbone opening y *vs.* z (see Fig. 1) were made on a number of defects. Typical results are plotted in figure 2 for the range of defect sizes over which

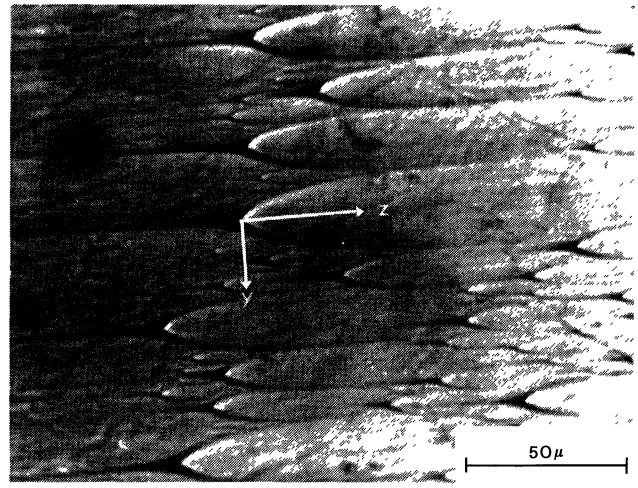

FIG. 1. — Transmission micrograph of parabolic focal conic defects obtained in parallel-oriented samples of smectic A CBOOA at $T = 78$ °C (Thickness = 125 μ).

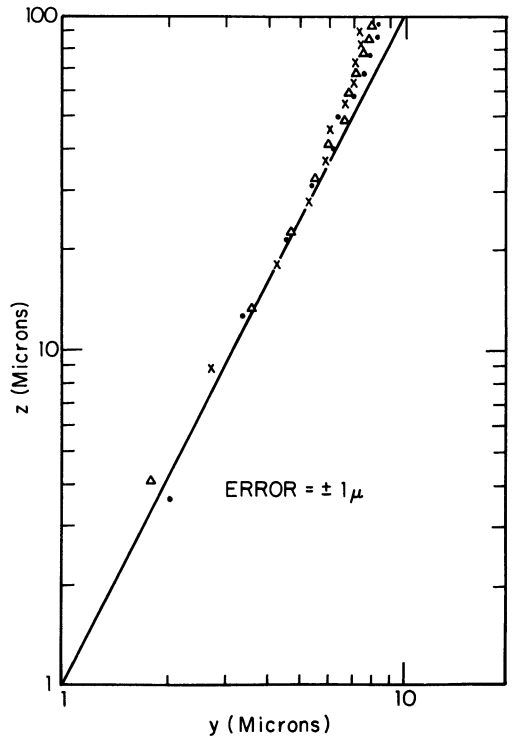

FIG. 2. — A log-log plot of wishbone spacing y *vs.* z for three sizes of defect. The horizontal axis of each data set is translated (i.e., y values scaled) to make the data asymptotic with $y = z^2$ for small z. Key : (●) $z = 0.086\,7\,y^2$; (Δ) $z = 0.130\,y^2$; (×) $z = 0.187\,y^2$; solid line represents $z = y^2$.

measurements could be made reliably. This range was limited on the lower end by optical resolution of the lines in small defects and on the higher end by the size of the largest defects found, which had focal lengths $f_{max} \sim 4$ μ for a sample thickness t of $t = 125$ μ. We found that f_{max} decreases with decreasing sample thickness down to $t = 2$ μ.

For $z \leqslant 30$ μ, the curves appear to be parabolic. At large y values deviations from this form were

observed with $(z - \alpha y^2)$ positive and increasing with increasing y in every case. For purposes of plotting figure 2, the y values of the three data sets were scaled to make each set asymptotic with $z = y^2$ for $z \lesssim 30$ μ. The actually asymptotic parabolae $z = \alpha y^2$ are also indicated in the figure caption. The focal lengths $f = (4\alpha)^{-1}$ of the asymptotic parabolae are 2.9 μ (•), 1.9 μ (Δ) and 1.3 μ (×). The deviations from parabolic shape at large z are evident beginning at roughly the same value of z for the different sized defects.

Further evidence for the nature of these defects came from adjusting the focus of the microscope. This showed that the parabolic line was generally in a plane parallel to the glass slides. The tail of the wishbone, however, appeared to be in focus a distance s above the plane of the parabola for a given defect ; s increased as $| - z |$ increased. Occasionally the parabola was somewhat tilted with respect to the slides, in which case the tail of the wishbone appeared to split into a narrow parabola. A similar effect occurred if the sample itself was tilted about the z axis. This suggested a possible structure consisting of intersecting parabolae oriented antiparallel and rotated 90° about the z axis with respect to each other (point group D_{2d}). The case in which the two line defects are identical parabolae passing through each other's foci appeared to be appropriate. We now discuss its geometry in detail.

3. **Parabolic focal conics (PFC's).** — We consider here an *ideal* smectic A phase (elastic compression constant $B = \infty$) in which layers are everywhere of thickness d. In such a structure, the only line disclinations are ideal focal conics. The smectic layers form a family of Dupin-cyclides, i.e., the envelope of spheres whose centers lie in a plane and are simultaneously tangent to two circles in that plane [5]. In particular, consider the case of two circles in the y-z plane, circle a having radius $= r_a$ and circle b having radius $r_b = \infty$ (a straight line) as indicated in figures 3*a*, *b*.

It can be shown that the spheres tangent to these two circles can also be specified by the combination of the circle of infinite radius and a parabola, as indicated in figures 3*a*, *b*. The generating spheres are then defined to have their centers on the parabola and to be tangent to the circle *b*. The enveloping surface so generated will define a layer of smectic liquid crystal.

Obtaining an equation for the surface of a smectic layer is straightforward. The parabola is defined as

$$z = \frac{y^2}{4f} - \frac{f}{2},$$

where f is its focal length.

With this choice of the parabola, and taking circle *b* to be located at $z = c$, circle *a* must be centered at $z = f/2$ and have a radius $r_a = c + 3f/2$. We then define a function $u(x, y, z_0)$ which is the displacement, parallel to z, of the point (x, y) on the smectic layer originally in the plane z_0 to its new position $[u(x, y, z_0) + z_0]$ in the same smectic layer (Fig. 3*b*). To obtain $u(x, y, z_0)$ we write the equation for the generating sphere centered about some point (y', z') on the parabola :

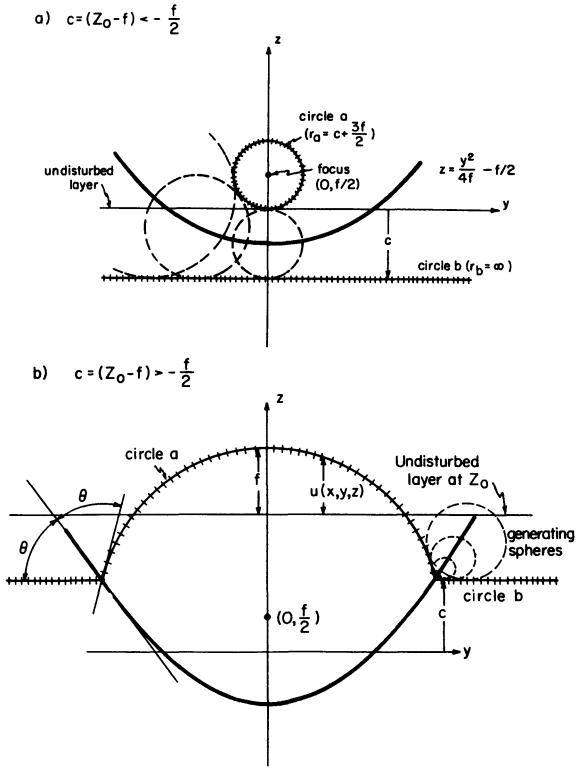

FIG. 3. — (*a*) Generating circles *a* and *b* and parabola for a typical case in which circles *a* and *b* do not intersect ($c < -f/2$). Dotted curves represent the generating spheres, the envelope of which is a smectic layer. For certain cases when circles *a* and *b* are non-intersecting, the smectic layer is multiply-connected in a bridge-tunnel arrangement. (See Fig. 4*b*, *c*.) (*b*) Same as (*a*) for case where circles *a* and *b* intersect. The distortion u of a smectic layer in the focal conic is defined such that $u = (\pm) f$ in the limit of large $\begin{pmatrix} x \\ y \end{pmatrix}$. Note formation of a conical cusp at the parabola.

$$r = \left[x^2 + (y - y')^2 + \left(z - \frac{y'^2}{4f} + \frac{f}{2}\right)\right]^{1/2}. \quad (1)$$

This radius is then set equal to the perpendicular distance from (y', z') to the line at $z = c$ and the resulting equation is solved for z. We then set $dz/dy' = 0$ and, together with the equation for z, eliminate the parameter y'. The resulting equation $F(x, y, z) = 0$ yields the roots $z(x, y)$. Upon making the required transformations $c = z_0 - f$ and $u = -f + z - c = z - z_0$, we find the following equation for $u(x, y, z_0)$:

$$F(u) = -(u + f)^3 + (u + f)^2 (3f - 2z_0) - \\ - (u + f)(x^2 + y^2 + 2f^2 - 4fz_0) + 2fx^2 = 0. \quad (2)$$

It is possible to generate a family of surfaces by varying the initial layer location z_0. There are three

distinct regions of z_0 to consider. For $z_0 \geqslant f/2$ the surface is singly connected (Fig. 4*a*). Slicing the surface with the $x = 0$ plane (Fig. 3*b*), one finds an arc of a circle (circle *a*) joining two semi-infinite line segments (circle *b*). The intersections form cusps, whose locus (with z_0 as parameter) represents the upward parabola. The cusps in a given smectic layer are conical, having cylindrical symmetry about a line tangent to the parabola where it intersects the layer. As $z_0 \to \infty$, the cusps tend to become less sharp, the cone angle θ varying approximately as $\theta \sim \frac{\pi}{2} - \sqrt{\frac{f}{z_0}}$ (Fig. 3*b*).

In the region $z_0 \leqslant -f/2$ we obtain a similar situation, where the system for $z_0 \geqslant f/2$ has effectively been rotated by $\pi/2$ about the symmetry (z) axis and by π about the x or y axis (Fig. *d*, *e*, *f*). It should be pointed out that for y values between the cusps, F has three real roots in the region $| z_0 | > f/2$. Two of these roots represent continuations of the circular arc and line segment (Fig. 4*f*) and are discarded.

The region for $-f/2 < z_0 < f/2$ is of some interest, since here the smectic layers are predicted to be multiply connected. To visualize what happens in this region, let us first consider the evolution of the layers as z_0 approaches $f/2$ from above, i.e., $z_0 > f/2$. As z_0 approaches $f/2$, the conical cusps on the parabola become sharper and closer together, until they finally meet at the point $(0, 0, -f/2)$ when $z_0 = f/2$ (Fig. 4*a*). As z_0 continues toward zero (Fig. 4*b*), a hole is poked through the sheet where the two cusps met, closing off the crest and thereby creating a bridge-tunnel combination. When z_0 passes through zero and becomes negative, the tunnel continues to grow and the bridge to shrink (Fig. 4*c*). Finally, at $z_0 = -f/2$, the bridge separates into the other pair of conical cusps (Fig. 4*d*).

In the parabolic focal conic then, the smectic layers curve smoothly except for the lines of point discontinuity forming conical cusps on the two parabolae. Because the smectic A phase is locally uniaxial with the optic axis normal to the layers, the cusps represent the regions of largest refractive index inhomogeneity. They are thus the observable feature of the defects. The complex structure at the core of the defect ($| z_0 | \lesssim f$) should also have some characteristic appearances under the microscope. This, however, was not observed because of the small dimension of the core region ($\sim 2f$) and because a dust particle was frequently located in the core.

We have now completed the presentation of the structure of ideal parabolic focal conic defects. Our microscopic observations detailed in section 2 lead us to the conclusion that the observed wishbone defect is a structure closely related to parabolic focal conics.

4. **Discussion.** — 4.1 ISOLATED PFC's. — For the general case of an isolated complete focal conic defect structure consisting of a confocal ellipse and hyperbola and the associated family of Dupin cyclides, for distances from the focal region large compared to the dimensions of the ellipse, the Dupin cyclides approach the form of spherical surfaces, with weak cusps where the hyperbola cuts the surface. In contrast, for an isolated PFC, the structure far from the focal region approaches flat smectic layers, in the sense that the

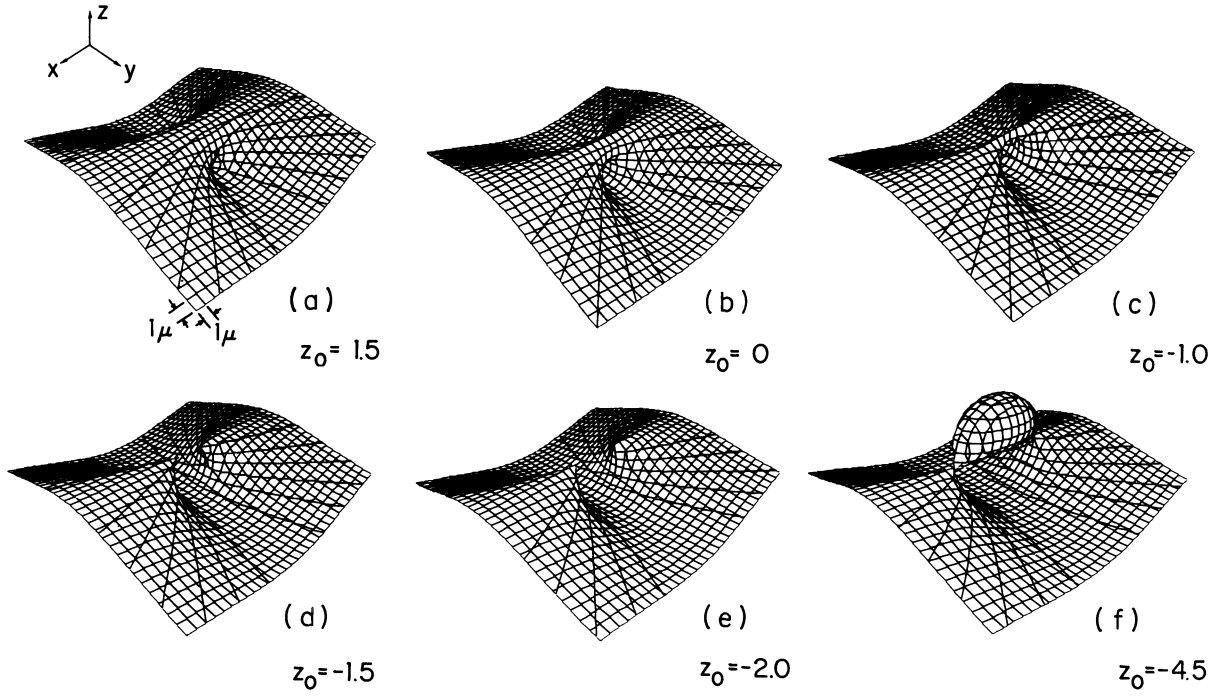

FIG. 4. — Computer plots of smectic layer surfaces for various values of z when $f = 3$ μ. The undistorted layer is an (x, y) plane located at z_0 half way between the surfaces of $x \to \infty$ and $y \to \infty$; lines drawn on surfaces are contours of constant u. For figure 4*d*, $z_0 = -f/2$, the cusps actually touch, although in the figure they do not appear to. This is a result of the digitizing process in the plotting routine. Fig. 4*f* shows an extraneous blob due to non-physical components of $F(u)$.

gradient of the layers approaches zero everywhere, with weak cusps defining the parabolae. Therefore it is easy for PFC's to exist as isolated defects in an otherwise planar smectic single crystal. The one other focal conic structure that is compatible with a planar sample is a hybrid structure described by another limiting case, in which the line defects are a circle and straight line normal to the center of the circle. In this case, if the Dupin cyclides are terminated at the surface of the right circular cylinder defined by the circular disclination, a smooth junction to flat layers outside this cylinder is possible [14]. The fact that PFC's are much more commonly observed in our samples than the circle line pairs might be explained by two facts. First, the generation of defects by stress relaxation, as discussed below, seems especially compatible with the PFC structure, while it is not obvious how it would be accomplished by circle-line defects. Second, a circle-line pair of visible size involves the interconnection, through the center of the circle of radius r, of a large number (r/d) of smectic layers ; in this sense it is a gross defect, difficult to generate from an initially planar sample. By contrast, the multiple connection of smectic layers in a PFC is confined to the small focal region, only of the order of a few microns in size for the largest PFC's we have seen.

4.2 INTERACTIONS OF PFC'S WITH BOUNDING SURFACES. — There is evidence from our observations that PFC's interact both with the boundary surfaces and with each other : (*a*) PFC's, even isolated ones, are nearly always found with one parabola oriented parallel to and the other normal to the confining plates (see Fig. 1) ; (*b*) larger PFC's tend to be found centered between the glass plates in the parallel samples ; (*c*) PFC's which have coplanar parabolae and are next to each other are always oriented with the coplanar parabolae extending in the same direction, as depicted in figure 5*a*. In an attempt to understand these effects, we have calculated the far field distortion of an ideal PFC, i.e.

$$u(x, y, z_0) \quad \text{for} \quad r = \sqrt{x^2 + y^2} \gg 2\sqrt{fz_0} .$$

In this limit we find, using eq. (1) :

$$\lim_{r \to \infty} u(x, y, z_0) \equiv \bar{u}(x, y, z_0) = \frac{(x^2 - y^2) f}{x^2 + y^2} \qquad (3)$$

so that $\bar{u}$ is independent of z_0 for large r. Using polar coordinates $(y = r \sin \theta, \quad x = r \cos \theta)$, $\bar{u}(x, y, z_0)$ becomes :

$$\bar{u}(\theta) = f \cos 2\theta .$$

The distortion in the ideal case does not die out for large r but approaches $+ f$ along the x axis and $- f$ along the y axis as $r \to \infty$, independent of z_0.

We have used this result to estimate in a very crude way the energy of interaction of an ideal PFC with a bounding plate enforcing parallel orientation. The geometry is shown in figure 6*a*. We assume an anisotropic surface energy at the plate, tending to orient molecules parallel to z, to be the dominant energy term. The surface energy E, per unit area, will be given by :

$$E = \frac{1}{2}\gamma_1\left(\frac{\partial u}{\partial y}\right)^2 + \frac{1}{2}\gamma_2\left(\frac{\partial u}{\partial x}\right)^2 . \qquad (4)$$

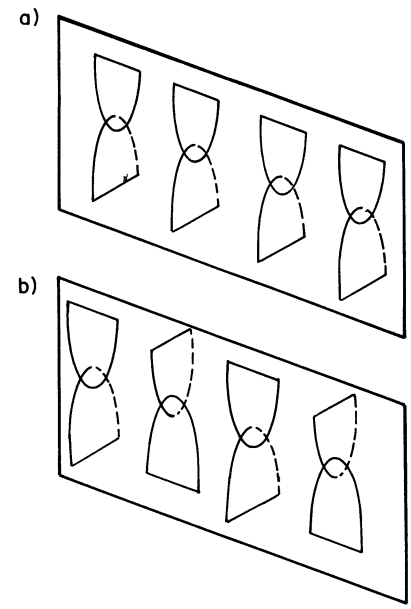

FIG. 5. — (*a*) Commonly observed arrangement of coplanar PFC's. (*b*) Not observed.

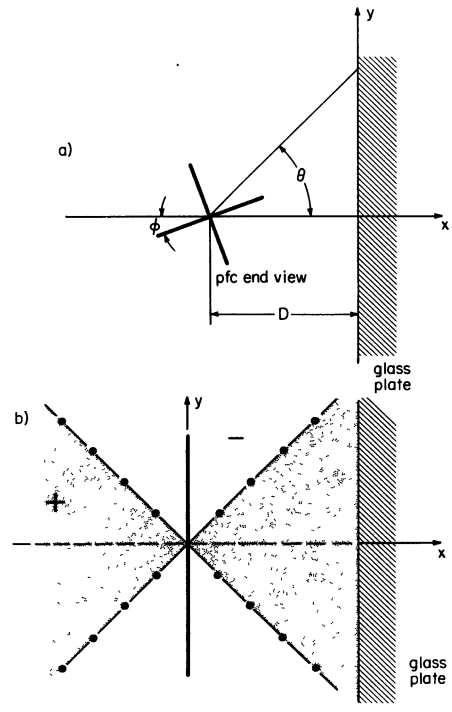

FIG. 6. — (*a*) Geometry for calculation of the interaction of a PFC with an orienting wall. The heavy lines indicate the planes of the parabolae. (*b*) Ideal defect oriented optimally with respect to wall according to observations. Shaded areas indicate positive $\bar{u}$ (layer is moved toward reader). Lines indicate as follows : (—●—●—) : $\bar{u} = 0$; (———) : $\partial\bar{u}/\partial\theta = 0$, $u = -f$ (upward parabola) ; (— — —) : $\partial\bar{u}/\partial\theta = 0$, $\bar{u} = +f$ (downward parabola). This geometry minimizes $(\partial\bar{u}/\partial\theta)^2$ at the wall close to the defect.

Assuming the far field layer distortion $\bar{u}(x, y)$ is that of the ideal PFC, the energy of interaction ε of the PFC with the wall, per unit length, in the z direction is given by :

$$\varepsilon = \frac{1}{2}\int_{-\infty}^{\infty} dy\left[\gamma_1\left(\frac{\partial\bar{u}(x, y)}{\partial y}\right)^2 + \gamma_2\left(\frac{\partial\bar{u}(x, y)}{\partial x}\right)^2\right] \quad (5)$$

$$= \frac{2f^2}{D}(\gamma_1 + \gamma_2)\,. \quad (6)$$

Eq. (6) shows that the PFC will experience a net force F, per unit length,

$$F = \frac{\partial\varepsilon}{\partial D} = -\frac{2f^2}{D^2}(\gamma_1 + \gamma_2)$$

away from the wall, independent of its orientation angle φ. Therefore, on the basis of this model, no argument can be made concerning the orientation of the defects. It should be noted, however, that the observed orientation ($\varphi = 0$) tends to reduce $\partial u/\partial y$ in the vicinity of $y = 0$, i.e., close to the PFC. This orientation is diagrammed in figure 6*b*, where the upward (downward) parabola opens toward (away from) reader.

From eq. (6) it is clear that a PFC between two plates will have minimum energy when located in the midplane. This model then correctly predicts that PFC's should be found near the center of the cell as we have observed under the microscope. Extending these considerations to more general cases presents some rather formidable difficulties. Any realistic calculation would have to include the effects of finite smectic layer compressibility as well as a layer distortion caused by the boundary conditions. This would be very difficult. It is clear from the PFC geometry, however, that the average molecular tilt angle away from the z axis increases as the center of the defect is approached. Hence, it seems likely that even in the most general case a PFC should be repelled by a boundary characterized by eq. (4).

4.3 MUTUAL INTERACTIONS. — The preferred arrangement of defects in an array should be that which minimizes elastic energy, which in turn is that which allows the easiest match-up of adjacent far field distortions. By this criterion we propose the fundamental arrangement indicated in figure 7*a*. It is in general agreement with our observation in parallel samples that coplanar PFC's are oriented in the same direction, since a row of PFC's in figure 7*a* would appear as in figures 7*b* and 5*a*. This fact, however, cannot be taken as evidence for the arrangement of figure 7*a* because of the influence of the bounding glass plates. In the perpendicular orientation, on the other hand, boundary effects in planes parallel to z are not of importance, and a test of the proposed arrangement of figure 7*a* is possible.

To this end we produced and studied focal conic

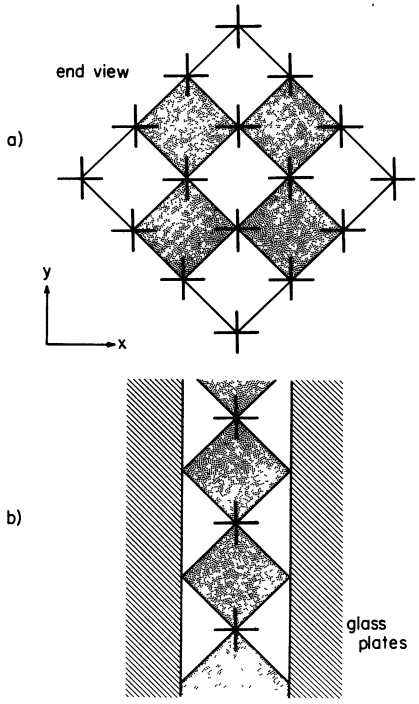

FIG. 7. — (*a*) Fundamental arrangement of PFC's in thick sample. (*b*) In thin parallel sample (typically observed in 125 μ sample).

arrays in single domain perpendicular CBOOA samples of thickness $t = 500$ μ. The focal conic arrays were generated by applying a dilative strain normal to the layers. The details of the generation process will be discussed in the next section. For a sufficiently large strain, the perpendicular sample, normally dark between crossed polarizers, began to transmit light, indicating a tilting of layers from the planar geometry. The transmitted intensity is characterized by a polygonal array of line defects [6]. This strain-induced polygonal array, which is also observable in cholesteric planar textures [4, 7], is a form of focal conic texture, but the exact structure has, until now, not been determined. We have observed the spatial arrangement of line defects in the polygonal array by tilting the sample and varying the microscopic plane of focus. On the basis of this study and of our understanding of PFC geometry, we propose for the ideal polygonal texture the line defect structure indicated in figure 9 — a square array of parabolic focal conics in which the PFC's join smoothly to each other to fill space. This arrangement is precisely that of figure 7*a*, which was arrived at on the basis of the easiest matching of PFC far field distortions, with the added feature that the parabolae of adjacent defects meet at the sample surfaces. This feature leads to the following relation for ideal PFC's of focal length f, sample thickness t, and parabola width at the surface $2R$:

$$f = \frac{R^2}{2t}\,. \quad (7)$$

Evidence for this arrangement is given in figures 8*a*, *b* which show transmission micrography between cross-

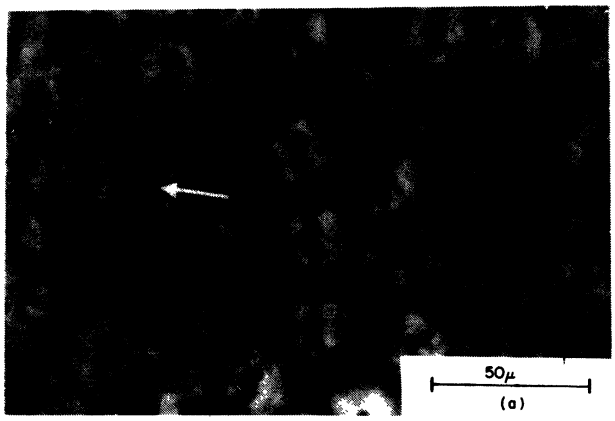

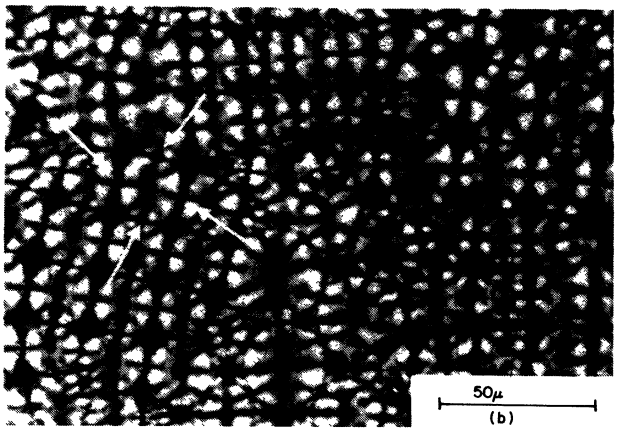

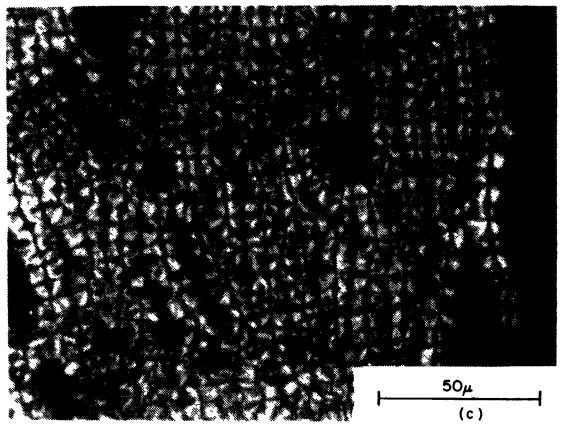

FIG. 8. — Photographs of perpendicular samples : (*a*) 500 μ thick sample of CBOOA in smectic phase. A large dilatation ($\delta d \gg 3\ \pi\lambda$) has created an array of PFC's. Here microscope is focussed at the top surface; the arrow indicates a typical convergence point of four parabolae. (*b*) Same as (*a*) except that focal plane is midway between slides; arrows indicate grid of the four PFC cores (crosses). (*c*) 125 μ thick sample of p-ethyloxybenzylidene-p-β-methylbutylaniline (EBMBA) in cholesteric phase; pitch = 2 000 Å.

ed polarizers of the defect structure with the microscope focussed at two heights in the sample. As the focus is moved down from the top of the sample, there appears at the top surface a regular array of black spots (Fig. 8*a*) produced by the intersections of the upward parabolae with the top surface (see Fig. 9). As the focus continues downward the cores of the defects

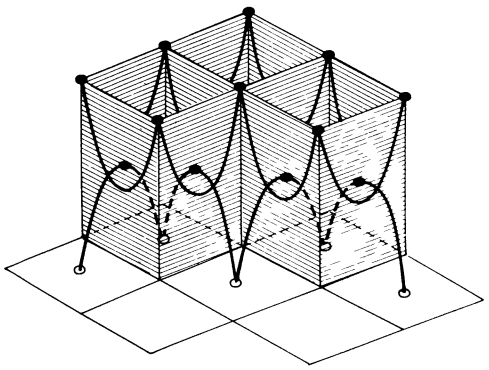

FIG. 9. — Three-dimensional structure of the four-fold grid pattern in figure 8.

come into focus; they appear as an array of crosses, with each crossbar on a line connecting two of the surface black dots (Fig. 8*b*). One bar comes into focus first with two sharp points moving into the center along it and then out on the other bar as the focal plane is lowered; this is as would be expected for the crossed parabola structure. With the sample parallel to the microscope stage, no further structure can be discerned as the focus is lowered. However, upon tilting the sample, the complementary array of dots on the bottom surface (see Fig. 9) can be brought into focus. This effect is probably a result of the optical distortion to be expected in such a thick, nonuniform, uniaxial system. Tilting also provides direct evidence for the PFC's in that upon tilting the crosses turn into wishbone-like structures. Finally, figure 8*c* depicts EBMBA in the cholesteric phase. Again the texture is essentially identical to the smectic A phase in figure 8*b*.

A PFC array will have the *ideal* square polygonal texture when all parabolae have the same width at the surface. This requires that the PFC's all have the same focal length and all have their cores in the sample midplane. Breakdown of these conditions leads to the disordered polygonal texture that is frequently observed. An example is diagrammed in figure 10, obtained from a photograph of a CBOOA smectic polygonal texture. The elements of this array, the PFC's, are shown in figure 10*a* (see caption for key). Note that a PFC not in the sample midplane will have different parabolae widths at the top and bottom surfaces, hence dashed and solid line segments of differing lengths. This array is quite typical, showing a small *ideal* region having solid and dashed segments of equal lengths between dots and forming a four-fold coordination at the dots. This *ideal* region is bounded by a less ordered array composed of PFC's with solid and dashed lines of unequal lengths, having from three-fold to six-fold coordination of the dots. The arrow indicates one such defect for which the upward parabola is wider at the top surface than the downward parabola is at the bottom surface. Hence the core of this PFC is in the bottom half of the sample. PFC's which are centered but are of larger focal length are

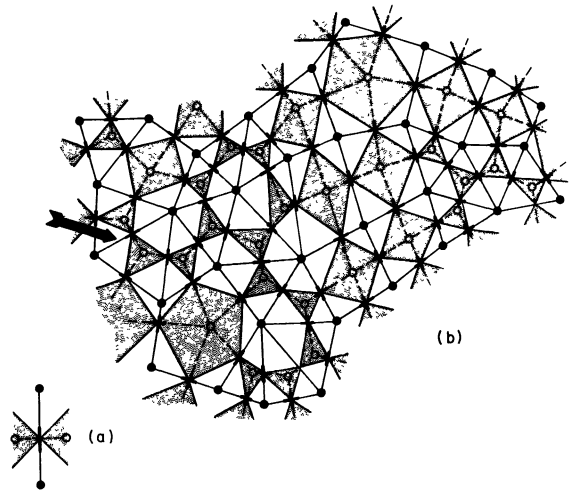

FIG. 10. — (*a*) Diagrammatic non-ideal PFC array element. Key : Heavy cross : PFC core ; solid lines (——) : upward opening parabola (toward reader) ; dashed lines (- - -) : downward opening parabola ; closed dots (●) : parabolae intersection at top surface ; open dots (○) : parabolae intersection at bottom surface ; shaded areas indicate layer displacement toward reader. Ideally the cross should be at the center of the dashed and solid line segments. (*b*) Typical non-ideal array of PFC's in smectic A CBOOA.

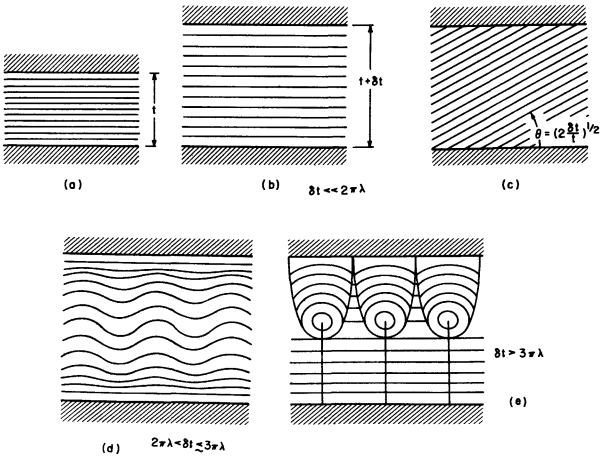

FIG. 11. — Evolution of layer distortion under applied dilation : (*a*) Initial equilibrium sample. (*b*) For $\delta d < \lambda$, layers simply dilate. They can, however, lower their dilative elastic energy by tilting as shown in (*c*). Uniform tilt, however, is not compatible with perpendicular boundary conditions ; hence, an undulating texture is assumed with a partial relaxation of dilative strain and the creation of splay distortion as shown in (*d*). For large strain (*e*) perpendicular boundary conditions break down slightly and splay distortion condenses to line disclinations in a PFC array ; this depicts a cut through a row of parabolae.

also evident. In general crosses are centered on their line segments, although some *stretching* is necessary, indicating that distortion of PFC's is energetically preferable to not having adjacent parabolae meet.

Another observation in a perpendicular sample supporting our picture of the polygonal structure and the rules governing interactions of PFC's is the occasional formation of an isolated row of defects ; this appears to be precisely the structure depicted in figure 5*a*, with one set of parallel parabolae meeting at a line of points along one of the sample surfaces. Such rows often exist as the last remnants of an array, and the spacing of the defects is approximately that observed in the array. On the other hand, we do not see stable isolated PFC's in perpendicular samples. The rare isolated defects appear to be circle-line structures, with the circle attached to one glass plate. They are probably associated with local imperfections in the surface treatment, allowing molecules to lie parallel to the surface in a small region.

To summarize, we believe that the polygonal texture which appears in a single domain smectic A upon dilation is a PFC array. We now turn to the question of why such a distortion should appear at all.

4.4 DILATIVE STRAIN RELAXATION BY PFC's. — The key feature of the generation of focal conic domains in single domain smectic A samples is that they are produced by dilative strain. The mechanism of generation is indicated in figure 11. Consider a smectic sample of N layers and thickness t between glass plates (Fig. 11*a*). If a dilative stress is applied so that $t \to t + \delta t$ ($\delta t \ll t$) and δt is sufficiently small, then a fractional expansion of each layer, $\delta d/d$ equal to $\delta t/t$ occurs (Fig. 11*b*). However, if the layers are fluid, they can flow over one another and tilt to relax the strain (Fig. 11*c*). A tilt through an angle θ such that

$$\sec\theta - 1 \cong \frac{1}{2}\theta^2 = \frac{1}{2}\left(\frac{\partial u}{\partial x}\right)^2 = \frac{\delta d}{d} \qquad (8)$$

will completely relax the dilative strain $\delta d/d$. Thus layers tilting through only very small angles can readily relax applied strains.

Because of the boundary conditions, $u(x, y) = 0$ at the glass plates, the simple tilt distortion of figure 11*c* is not possible at small $\delta t/t$, and tilt can be achieved only at the expense of layer curvature ; this curvature is associated with splay elastic energy :

$$E_s = \frac{1}{2} K \left[\frac{\partial^2 u}{\partial x^2} + \frac{\partial^2 u}{\partial y^2}\right]^2 .$$

Here K is the Frank splay elastic constant. The layer distortion to be expected is obtained via a minimization of the total (dilative + splay) elastic energy :

$$U = \int dV \left[\frac{B}{2}\left\{\frac{\partial u}{\partial t} - \frac{1}{2}\left[\left(\frac{\partial u}{\partial x}\right)^2 + \left(\frac{\partial u}{\partial y}\right)^2\right]\right\}^2 + \frac{K}{2}\left(\frac{\partial^2 u}{\partial x^2} + \frac{\partial^2 u}{\partial y^2}\right)^2\right] \qquad (9)$$

B is the compressional elastic constant.

Minimization leads to the prediction of a dilation-induced undulation instability [6, 8], wherein for $\delta t < \delta t_c = 2\pi\lambda = 2\pi\sqrt{K/B}$, the layer distortion to be expected is that indicated in figure 11*b* — simple dilation. For $\delta t > \delta t_c$, however, the distortion is of the

form depicted in figure 11*d* — dilation plus a layer undulation $\delta u(x, y, z_0)$ [9],

$$\delta u(x, y, z_0) = u_0 \cos \frac{\pi}{t} z \cos \frac{q_c}{\sqrt{2}} x \cos \frac{q_c}{\sqrt{2}} y \quad (10)$$

$$u_0 = \frac{4\sqrt{2}}{3} \lambda[(\alpha - \alpha_c)/\alpha_c]^{1/2} \quad (11)$$

$$q_c = (\pi/\lambda t)^{1/2}; \qquad \alpha = \delta t/t, \qquad \alpha_c = \delta t_c/t. \quad (12)$$

Hence, for $\delta t > \delta t_c$, the layers tilt to achieve a partial strain relaxation in some regions. The key features of this model are borne out by experiment for $0 < \delta t \lesssim 1.5\, \delta t_c$ [10, 6].

For $\delta t \gtrsim 1.5\, \delta t_c$, on the other hand, a second instability occurs which is not predicted by the above model. This second instability is characterized by the appearance of the polygonal focal conic texture, indicated schematically in figure 11*e*. From the discussion of the previous section we have identified this structure as a PFC array.

Several important changes are associated with the appearance of the PFC array. The continuously distributed splay deformation partially condenses into localized disinclinations. Just how much this changes the free energy is hard to calculate precisely. Probably more important, the transition to a PFC array relaxes dilative strains, the increased total sample thickness being accommodated by the increased average layer tilt and by the change in the number of layers due to the multiple connectivity of layers in the PFC core region. At the same time it appears that the perpendicular boundary conditions are slightly relaxed and that in the vicinity of the points where parabolas meet there are some smectic layers which terminate probably at the surfaces. Figure 12 depicts the PFC array whose average distortion pattern matches the two dimensional undulation structure. Figure 13 shows the change in conformation of a pair of typical smectic layers located symmetrically above and below the midplane of the sample, near the surfaces. Where four parabolas almost meet, the shape of a smectic layer resembles the groined arch of a vaulted ceiling.

One of the features of the continuous undulation pattern is that the smectic layers in contact with the surfaces before dilation remain in contact with them. It would be interesting to see if this condition is preserved through the transition to a PFC array. This would require $\delta t = 2\, f$. If we assume that the period of the PFC array matches that of the undulation pattern, then the characteristic half width of the parabolas at the surfaces is

$$R_0 = \frac{\pi}{q_c} = (\pi \lambda t)^{1/2}. \quad (13)$$

From the equation for the parabola,

$$R_0 \cong (2\, ft)^{1/2}. \quad (14)$$

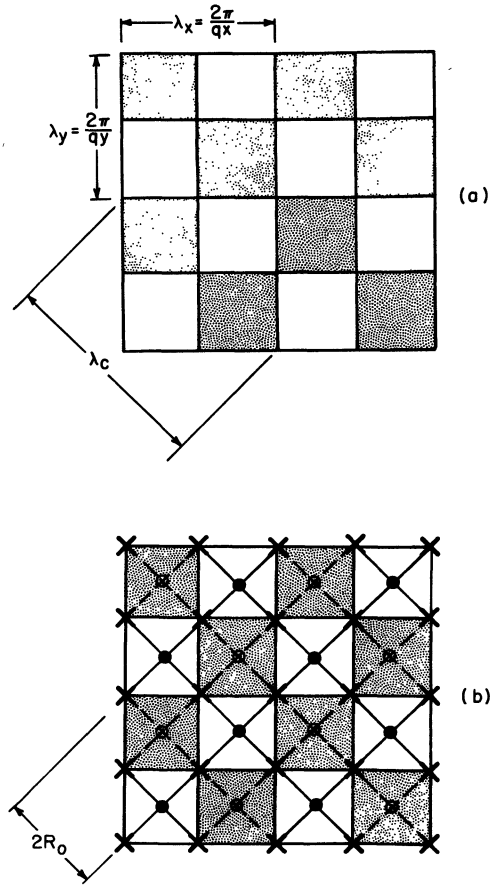

FIG. 12. — Diagram of layer distortion in the undulating texture (a) and distortion in the PFC array whose far field distortion matches the undulations. See figure 10 for key.

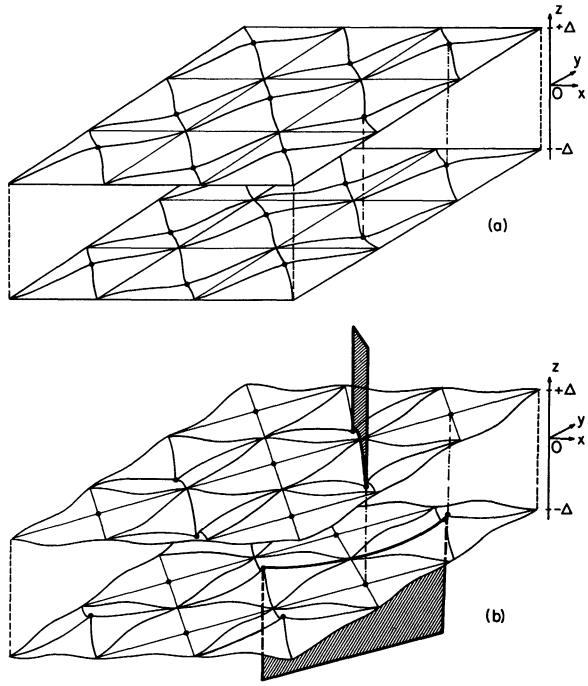

FIG. 13. — Distortion of layers in the vicinity of the sample surface (i.e., $\Delta \sim t/2$). (*a*) In the crossed undulation texture. (*b*) In the matching PFC texture. Shaded planes indicate location of parabola in a PFC.

Then,

$$f = \frac{\pi}{2}\lambda\,. \tag{15}$$

If the PFC array appears at $\delta t \sim 1.5\, t_c = 3\,\pi\lambda$, then

$$2\,f = \frac{1}{3}\delta t\,, \tag{16}$$

in contrast to the conjecture that $2\,f = \delta t$. The geometry of the PFC array scales with sample thickness in the same way as the undulation instability, making the two structures reasonably compatible. The discrepancy between the value of f estimated from the period of the array and that estimated from the boundary condition proposed above might be explained in three ways. First, the parabolae may meet precisely at the surface, as we have proposed, and there is still some residual dilative strain just after they form. Or, a few extra layers may have been generated to account for the difference between $2\,f$ and δt; only a few are required, since δt is only of the order of a few layers thickness anyway. Or, in fact $2\,f$ may equal δt, and the parabolae could meet before reaching the sample surfaces.

This last possibility is not unreasonable. As is clear in figure 1, pairs of neighbouring parabolae tend to meet and continue together as a single line. The same could happen to four. This would tend to reduce the core energy of the disclination array. After the four parabolae had joined into one disclination, the smectic layer structure around the line would probably evolve from four-fold symmetric to cylindrically symmetric, closely resembling the structure around the straight line disclination of a circle-line focal conic pair. The observations necessary to test this speculation would have to be very precise. One point in support of it is that as δt changes, we should find $R_0 = \sqrt{t\,\delta t}$; in the non-periodic arrays, we do see a small increase in the mean R_0, as δt is increased.

The foregoing discussion presents a mechanism for relaxation of dilative strains in the planar smectic A texture which is both self-consistent and accounts for the observations, but which is also speculative and not precisely quantitative. The quantitative features are based on the assumption that the PFC's are ideal, i.e., that the line defects are parabolic. In figure 2 and the related text this has been shown not to be true. A better treatment of strain relaxation by PFC's would have to include a calculation of the exact line defect structure. We believe that the deviation of PFC structure from the parabolic shape is a result of the finite layer compressional elasticity (B finite), allowing an ideal PFC to relax some splay distortion at the expense of layer dilation.

De Gennes has calculated [11] the effect of finite B on the structure of a conical cusp, showing a core region of high splay and dilative energy to have a radius $r_c = 2\,\lambda/(\pi/2 - \theta)$, where cone angle θ is indicated in figure 3*b*. This result is relevant to the present discussion in several ways. First, it indicates that the overlap of adjacent parabolae near the surfaces in the PFC arrays (see Fig. 9) would eventually occur as they approached within r_c of one another. The *flattening* of the line defects from their parabolic shape at large z should make such overlap very effective in reducing core energy and may in fact result from the effective attraction between cores. Second, De Gennes' result allows an estimation of the visibility of the line defects, if the assumption is made that to be visible a cusp has to have a radius of curvature $r_c \lesssim \lambda_V/2$, where λ_V is the optical wavelength employed in the medium. With this assumption cusps, and hence the parabolae, will be visible (Fig. 1) as long as :

$$\frac{dy}{dz} = \frac{\pi}{2} - \theta \gtrsim \frac{4\,\lambda}{\lambda_V} \sim \frac{4(2.0\text{ nm})}{300.0\text{ nm}} \sim 3 \times 10^{-2}$$

where $z(y)$ gives the cusp location. Measurement of $z(y)$ and observation of line visibility (Section 2.2) showed this estimate to be a reasonable one. An ideal parabola on the other hand has $dy/dz \sim 3 \times 10^{-2}$ at $z \simeq 4\,000\,f$. For $f = 1\,\mu$, the parabola would be visible for up to $z \sim 4$ mm [12]. It also seemed possible that the deviation from parabolic shape of the PFC's in the parallel sample arose from an imperfect degeneracy, i.e., that the line parallel to the glass plates is an ellipse of large but finite major axis. However, calculation shows that any ellipse having the correct parabolic asymptotic behaviour at small z ought to be visible out to very large z ($|\,z\,| \sim 3$ mm). Hence the observed visibility to only $|\,z\,| \sim 300\,\mu$ should eliminate this possibility.

The picture presented so far is based on the observation of metastable defect arrays and the conditions necessary for their appearance. The detailed dynamics of their appearance is hard to observe, but the gradual disappearance of an array is easily studied. It occurs by the growth of perfect homeotropic regions bounding the array. The boundary is sharply defined, and moves by the sudden disappearance of individual PFC's along the boundary. This behaviour supports the general view, essential to the entire discussion, that the interaction between PFC's is not nearly as strong as would have been predicted from the strict geometrical view of focal conic arrays. The fact that an individual PFC can disappear without greatly disturbing its neighbours indicates a basic plasticity of the structure, which may be due to the existence and high mobility of sub-visible defects such as dislocations.

Finally, in addition to the evidence obtained from microscopy for the [undulation → PFC] transition, a dramatic change in the light scattering from smectic layer distortion for $\delta t \gtrsim 1.5\, t_c$ is observed. In the undulating texture one observes a single cone of scattered light. This corresponds to scattering with a small change in the z component of wave vector, i.e., $\Delta K_z = \{(K_{\text{incident}})_z - (K_{\text{scattered}})_z\} \sim \pi/t$ [13, 6]. For large δt, however, the cone splits and several rings of scattered light are observed, corresponding to

$\Delta K_z \gg \pi/t$. It seems likely that this effect will be understood in terms of the structure of the PFC texture and calculations are being carried out to test this point.

5. **Conclusion.** — We have presented evidence for, and a detailed discussion of, the structure of parabolic focal conics, a hitherto neglected form of focal conic defect, which we observe commonly in nearly perfect smectic samples. We have shown, by means of qualitative physical and geometrical arguments, that PFC's are the primary macroscopic defect structures which can be generated from a planar smectic A or cholesteric texture ; they are consequently the principal dilative strain relaxation mechanism for large strains in such systems.

Several aspects of this problem present fruitful avenues for further study. First, there is the question of the effect of finite layer compressibility on the defect structure, the understanding of which will make geometric arguments more precise. Second, we do not at this time have an elastic theory which will predict the kind of splay condensation that we have observed. Development of the appropriate non-linear equations would be most useful. Third, the idea that interaction between macroscopic focal conic defects is mediated in part by other sub-visible defects such as dislocations should be investigated further. Fourth, it would seem that a light scattering study of the PFC array would offer one means of obtaining information on its generation and growth. Finally, a comparative study of the polygonal arrays described here with those discussed by Bouligand would be very interesting. The macroscopic features of the two kinds of array are remarkably similar, but their internal structures are completely different. It should be especially illuminating to compare the conditions necessary for the generation of the two types of arrays.

Acknowledgments. — Support for this work has been provided by the National Science Foundation under contracts DMR76-22452 and DMR76-01111, by the Joint Services Electronics Program, and by the Division of Engineering and Applied Physics, Harvard University. The authors wish to thank Michael Archuleta of Lawrence Livermore Laboratory for the computer graphics (Fig. 4) used in this paper and Professor P. S. Pershan for many useful discussions.

References

[1] GRAY, G. W., *Molecular Structure and the Properties of Liquid Crystals* (Academic Press, London) 1962.
[2] BROWN, G. H. and SHAW, G. H., *Chem. Rev.* **57** (1957) 1049.
[3] BIDAUX, R., BOCCARA, N., SARMA, G., DESEZE, L., DE GENNES, P. G. and PARODI, O., *J. Physique* **34** (1973) 661.
[4] BOULIGAND, Y., *J. Physique* **33** (1972) 715.
[5] JESSOP, C. M., *Quartic Surfaces* (Cambridge University Press, Cambridge) 1916.
[6] RIBOTTA, R., *Etude Expérimentale de l'Elasticité des Smectiques*, Ph. D. Thesis, Université de Paris-Sud, Orsay (1975).
[7] RONDELEZ, F., *Contribution à l'étude des Effets de Champ dans les Cristaux Liquides Nématiques et Cholestériques*, Ph. D. Thesis, Université de Paris-Sud, Orsay (1973) ; RONDELEZ, F. and ARNOULD, H., *C. R. Hebd. Séan. Acad. Sci.* **273B** (1971) 549.
[8] CLARK, N. A. and MEYER, R. B., *Appl. Phys. Lett.* **22** (1973) 493.
[9] DELRIEU, J. M., *J. Chem. Phys.* **60** (1974) 1081.
[10] DELAYE, M., RIBOTTA, R., DURAND, G., *Phys. Lett.* **44** (1973) 139 ; CLARK, N. A., *Phys. Rev.* A **14** (1976) 1551.
[11] DE GENNES, P. G., *C. R. Hebd. Séan. Acad. Sci.* **275B** (1972) 549.
[12] We thank one of the referees for pointing out that GRANDJEAN, F., considered this problem : *Bull. Soc. Fr. Mineral.* **42** (1919) 42.
[13] CLARK, N. A. and PERSHAN, P. S., *Phys. Rev. Lett.* **30** (1973) 3 ; RIBOTTA, R., DURAND, G., LITSTER, J. D., *Solid State Commun.* **12** (1973) 27.
[14] We thank one of the referees for pointing out that more general hybrid structures exist, in which the parts of the Dupin cyclides with negative Gaussian curvature are joined to two sets of flat smectic layers oriented normal to the asymptotes of the hyperbolae. The eventual joining of these two sets of layers requires other defects, usually an array of similar focal conic pairs. Therefore these hybrid structures are not models for isolated defects in the interior of an otherwise perfect sample. See KLÉMAN, M., *Proc. R. Soc.* A **347** (1976) 387.